

Essential criteria for efficient pulse amplification via Raman and Brillouin scattering

R.M.G.M. Trines,¹ E.P. Alves,^{2,3} E. Webb,¹ J. Vieira,² F. Fiúza,³ R.A. Fonseca,^{2,4}
L.O. Silva,² J. Sadler,⁵ N. Ratan,⁵ L. Ceurvorst,⁵ M.F. Kasim,⁵ M. Tabak,⁶ D.
Froula,⁷ D. Haberberger,⁷ P.A. Norreys,^{5,1} R.A. Cairns,⁸ and R. Bingham^{1,9}

¹*Central Laser Facility, STFC Rutherford Appleton Laboratory,
Didcot, OX11 0QX, United Kingdom*

²*GoLP/IPFN, Instituto Superior Técnico,
Universidade de Lisboa, 1049-001 Lisbon, Portugal*

³*SLAC National Accelerator Laboratory, Menlo Park, CA 94025, USA*

⁴*DCTI/ISCTE Lisbon University Institute, 1649-026 Lisbon, Portugal*

⁵*Department of Physics, University of Oxford,
Oxford OX1 3PU, United Kingdom*

⁶*Lawrence Livermore National Laboratory, Livermore, CA 94550-9234, USA*

⁷*Laboratory for Laser Energetics, 250 East River Road, Rochester, NY 14623-1299, USA*

⁸*University of St Andrews, St Andrews, Fife KY16 9AJ, United Kingdom*

⁹*SUPA, Department of Physics, University of Strathclyde,
Glasgow, G4 0NG, United Kingdom*

(Dated: February 3, 2020)

Abstract

Raman and Brillouin amplification are two schemes for amplifying and compressing short laser pulses in plasma. Analytical models have already been derived for both schemes, but the full consequences of these models are little known or used. Here, we present new criteria that govern the evolution of the attractor solution for the seed pulse in Raman and Brillouin amplification, and show how the initial laser pulses need to be shaped to control the properties of the final amplified seed and improve the amplification efficiency.

Raman (and later Brillouin) scattering and amplification were first discovered in solid-state physics [1] and also found applications in gases and molecular vibrations [2–6] as well as non-linear optics [7, 8]. Raman and Brillouin scattering have also been demonstrated in laser-plasma interaction, see e.g. Forslund *et al.* [9]. Plasma-based compression and amplification of laser pulses via Raman or Brillouin scattering has been proposed to overcome the intensity limitations posed by solid-state optical systems [10–16]. In the context of Raman or Brillouin amplification, analytical models have been derived under the assumption that the basic shape of the growing seed pulse does not change during amplification, while its amplitude and duration evolve according to well-defined scaling laws [15, 16]. For Raman amplification (or Brillouin amplification in the weak-coupling regime), this assumption is only correct if the seed pulse has the following properties: (i) pulse amplitude is proportional to the interaction time t [17–21], (ii) pulse duration is proportional to $1/t$, or bandwidth proportional to t [18–22], (iii) pulse energy is proportional to t , or inversely proportional to its duration [23–28], (iv) the asymptotic “ π -pulse” solution is an attractor solution, i.e. a “not quite ideal” seed pulse will reshape itself into an approximate π -pulse shape [15, 19, 22, 28–33], (v) in multi-dimensional simulations where the pulses have a finite transverse width, the seed pulse acquires a “horseshoe” shape [18, 33–40]. Most of the above also applies to Brillouin amplification in the strong-coupling regime [16], although the scalings for the seed pulse duration and amplitude with interaction time are different. In this Letter, we perform the first detailed and systematic study of the full non-linear evolution of the seed pulse for both Raman and Brillouin amplification, and derive novel criteria for the optimal shape of the initial seed pulse before, during and after the interaction, which can be exploited to guide the design of future experiments and maximize their efficiency. At present, the properties of the ideal attractor solution for the seed pulse are not used to optimize the design of Raman or Brillouin amplification experiments.

We define a_0 and a_1 to be the scaled envelopes of pump and seed pulse respectively, $a_{0,1} \equiv 8.55 \times 10^{-10} g^{1/2} (I_{0,1} \lambda_{0,1}^2 [\text{Wcm}^{-2} \mu\text{m}^2])^{1/2}$, where $g = 1$ ($g = 1/2$) denotes linear (circular) polarisation. Let ω_0 and n_{cr} denote the pump laser frequency and critical density, and n_e and ω_{pe} the background electron density and corresponding plasma frequency. The group velocity of the pump pulse is $v_g = c^2 k_0 / \omega_0 = c(1 - n_e/n_{cr})^{1/2}$ and the electron thermal velocity is $v_e = (k_B T_e / m_e)^{1/2}$.

For Raman amplification, the envelope equations for pump, seed and plasma wave take

the following form [15]:

$$(\partial/\partial t \pm v_g \partial/\partial x)a_{0,1} = \mp i\Gamma_R a_{1,0} b^{(*)}, \quad (1)$$

$$(\partial/\partial t + 3v_e^2(k/\omega_{pe})\partial/\partial x)b = -i\Gamma_R a_0 a_1^*, \quad (2)$$

where $\Gamma_R a_0$ denotes the Raman backscattering growth rate in homogeneous plasma and $b \equiv \alpha_R \delta n_e / n_e$ with δn_e the envelope of the electron density fluctuations driven by the beating of pump and seed pulses, and α_R to be determined. Comparing these equations to the envelope equations by Forslund *et al.* [9] yields $\Gamma_R \alpha_R = \omega_{pe}^2 / (4\omega_0)$ and $\Gamma_R / \alpha_R = c^2 k^2 / (4g\omega_{pe})$, where $k \approx 2k_0 \approx 2\omega_0/c$ is the wave number of the RBS Langmuir wave (for $\omega_{pe} \ll \omega_0$). Then $\Gamma_R = [\omega_0 \omega_{pe} / (4g)]^{1/2}$ and $\alpha_R = \sqrt{g}(\omega_{pe}/\omega_0)^{3/2}/2$, with (1)-(2) valid for $a_0 < a_{wb} = \alpha_R / \sqrt{2}$ [15].

Following Malkin, Shvets and Fisch [15], or Menyuk, Levi and Winternitz [6], we define $\zeta = x/c + t$, $t' = \Gamma_R^2 a_{00}^2 t$ and $\xi = 2\sqrt{\zeta t'}$ where a_{00} denotes the pump pulse amplitude. Attractor solutions to the above system can then be obtained in terms of ξ alone. In particular, the first peak of the growing seed pulse can be approximated by $a_1(\zeta, t') \approx (2t'/\Gamma_R \xi) \partial u(\xi) / \partial \xi$ where $u(\xi) = 2\sqrt{2} \arctan[\epsilon \exp(\xi) / (4\sqrt{2\pi\xi})]$, with $\epsilon < 0.1$ depending on the initial seed pulse B-integral. The function $\partial u(\xi) / \partial \xi$ has an amplitude $A \approx 1.29$ and a width $\Delta\xi \approx 2.65$, mostly independent of ϵ , while the position of its maximum, ξ_M , obeys $5 < \xi_M < 7$ for practical values of ϵ [15, 18]. Let $\Delta\zeta$ denote the width of the first peak of $a_1(\zeta, t')$ for fixed t' and let $\xi_{1,2} = \xi_M \pm \Delta\xi/2$. Then $\xi_M \Delta\xi = (\xi_2^2 - \xi_1^2)/2 = 2t' \Delta\zeta$. For $\xi = \xi_M$, we find that $\|a_1\| = 2At' / (\Gamma_R \xi_M)$, $\Delta\zeta = \xi_M \Delta\xi / (2t')$. We consider pump and seed pulses with durations τ_0 and τ_1 (after amplification), and setting $\Delta\zeta = \tau_1$ and $t = \tau_0/2$ (for an interaction time t , the counter-propagating seed pulse consumes $2t$ of pump pulse), we find:

$$\Gamma_R^2 a_{00}^2 \tau_0 \tau_1 = \xi_M \Delta\xi \approx 15, \quad (3)$$

$$\Gamma_R \|a_1\| \tau_1 = A \Delta\xi \approx 3.4. \quad (4)$$

The asymptotic energy transfer efficiency for the first peak is then given by $\eta = \|a_1\|^2 \tau_1(t) / (2a_0^2 t) = A^2 \Delta\xi / \xi_M \approx 4.4 / \xi_M$. Thus, η is constant for a given configuration, and decreases with increasing ξ_M . We confirm these predictions in our simulations below.

The purpose of these equations is as follows. Eq. (3) allows one to derive scalings for the seed pulse duration $\tau_1(t)$ and amplitude $a_1(t)$, and also to tune these parameters via the

intensity of the pump pulse [33]. Eq. (4) provides a relationship between seed pulse duration and amplitude that does not depend on the pump pulse at all (the only combination of a_1 and τ_1 with this property). This is important for the tailoring of the initial seed pulse in experiments: $\tau_1(0)$ and $a_1(0)$ are not independent parameters, but should obey Eq. (4) for optimal energy transfer, otherwise the seed pulse will first reshape itself and only be amplified after that [30–33], reducing the amplification efficiency.

Brillouin scattering in the so-called weak-coupling regime [9, 12, 14, 41–43] is very similar to Raman scattering and can be treated in the same way. We introduce $\omega_{pi} = \omega_{pe} \sqrt{Zm_e/m_i}$ and $c_s = v_e \sqrt{Zm_e/m_i}$. For $a_{00}^2 < 8g(\omega_0/\omega_{pe})^2 c_s v_e^2 / c^3$, the electron pressure is the dominant restoring force and the plasma wave dispersion is not significantly affected by the beating between pump and seed pulses. In that case one can reuse equations (1)-(2) and only needs to replace $3v_e^2(k/\omega_{pe})$ by c_s in (2). For backward Brillouin scattering, the ion-acoustic wave has wave number $k_s = 2k_0$ and frequency $\omega_s = c_s k_s = 2c_s k_0$. Then we find $\Gamma_B \alpha_B = \omega_{pe}^2 / (4\omega_0)$ and $\Gamma_B / \alpha_B = c^2 c_s^2 k_s^2 / (4g\omega_s v_e^2)$, leading to $\Gamma_B = c\omega_{pe}\omega_s / (4v_e \sqrt{g\omega_0\omega_s})$ and $\alpha_B = \sqrt{g}v_e\omega_{pe} / (c\sqrt{\omega_0\omega_s})$. After substituting Γ_B, α_B for Γ_R, α_R , all the above results for Raman amplification also apply to the weak-coupling Brillouin case, including Eqns. (3) and (4), the wave breaking threshold $a_{wb} = \alpha_B / \sqrt{2}$, the numerical constants $5 < \xi_M < 7$, $\Delta\xi \approx 2.65$ and $A \approx 1.29$, and the seed pulse scalings.

For $a_{00}^2 > 8g(\omega_0/\omega_{pe})^2 c_s v_e^2 / c^3$ or $\Gamma a_0 / \omega_0 > c_s / c$, the ponderomotive pressure from the beating between pump and seed pulses will take over from the thermal pressure as the primary restoring force for the ion-acoustic wave. In this regime, called *strong-coupling* (sc) Brillouin scattering, the equation for the plasma wave becomes [16]:

$$\partial^2 b / \partial t^2 = -\alpha_{sc} c^2 k^2 \omega_{pi}^2 / (2g\omega_{pe}^2) a_0 a_1 = -\Gamma_{sc}^2 a_0 a_1. \quad (5)$$

From (1) and (5) and using $k = 2k_0 = 2\omega_0 v_g / c^2$ as before, we find: $\Gamma_{sc} \alpha_{sc} = \omega_{pe}^2 / (4\omega_0)$ and $\Gamma_{sc}^2 / \alpha_{sc} = c^2 k^2 \omega_{pi}^2 / (2g\omega_{pe}^2)$. This yields [9, 16, 44]:

$$\Gamma_{sc} = [(v_g/c)^2 \omega_{pi}^2 \omega_0 / (2g)]^{1/3} = (2\omega_s \Gamma_B^2)^{1/3}, \quad (6)$$

$$\Omega_{sc} = \omega_{sc} + i\gamma_{sc} = [(1 + i\sqrt{3})/2] \Gamma_{sc} a_{00}^{2/3}, \quad (7)$$

where ω_{sc} and γ_{sc} denote the frequency and growth rate of the ion-acoustic wave. Following the approach by Andreev *et al.* [16], we define $t' = \Gamma_{sc} a_{00}^{2/3} t$, $\zeta = \Gamma_{sc} a_{00}^{2/3} (t + x/v_g)$ and $\xi = \zeta \sqrt{t'}$. Again, attractor solutions to the system (1) and (5) can be obtained in terms of ξ

alone. In particular, the resulting seed pulse will scale as $a_1(\zeta, t') = a_{00}(t')^{3/4}f(\xi)$ where $f(\xi)$ has a fixed duration $\Delta\xi \approx 3.3$ and an amplitude $A \approx 0.62$ [16, 32]. Using $\Delta\xi = (\Delta\zeta)\sqrt{t'}$ for fixed t' , $\|a_1\| = a_{00}A(\Delta\xi/\Delta\zeta)^{3/2}$ and inserting $\Delta\zeta = \Gamma_{sc}a_{00}^{2/3}\tau_1$ and $t' = \Gamma_{sc}a_{00}^{2/3}\tau_0/2$ for pump and seed pulses with durations τ_0 and τ_1 into $\Delta\xi$ yields:

$$\Gamma_{sc}^3 a_{00}^2 \tau_0 \tau_1^2 = 2(\Delta\xi)^2 \approx 22, \quad (8)$$

$$\Gamma_{sc}^3 \|a_1\|^2 \tau_1^3 = A^2 (\Delta\xi)^3 \approx 13.8. \quad (9)$$

The scaling for the seed pulse duration is then $\tau_1(t) = \Delta\xi/(\Gamma_{sc}^{3/2}a_{00}t^{1/2})$, and the asymptotic efficiency is $\eta = a_1^2(t)\tau_1(t)/(2a_{00}^2t) = A^2\Delta\xi/2 \approx 0.63$. The role of (8) and (9) matches that of (3) and (4) for Raman amplification.

To verify the validity of Eqns. (4) and (9), we have carried out one-dimensional particle-in-cell simulations using the codes XOOPIC [45] and OSIRIS [46]. We used a long pump laser beam with constant amplitude a_0 and wave length $\lambda_0 = 1 \mu\text{m}$ ($\omega_0 = 2\pi c/\lambda_0$, $n_{cr} = \varepsilon_0 m_e \omega_0^2 / e^2$), a long plasma column with constant electron density n_0 and plasma frequency ω_{pe} , and a seed pulse with initial amplitude $a_1(0) = a_0$ and duration $\tau_1(0)$. For the Raman simulations, we used a plasma density corresponding to $\omega_{pe}/\omega_0 = 1/15$, pump laser amplitudes $a_{wb}/4$, $a_{wb}/2$, $3a_{wb}/4$, a_{wb} and $2a_{wb}$, with a_{wb} adjusted for each plasma density, and pump pulse durations up to $2 \times 10^5/\omega_0 \approx 112$ picoseconds. We use $\tau_1(0)/\tau_R = 0.1, 0.5, 1.0$ and 2.0 , where $\tau_R[\text{s}] = 4.22 \times 10^{-6} \lambda_0[\mu\text{m}](n_e/n_{cr})^{-1/4}(I_1 \lambda_1^2[\text{Wcm}^{-2}\mu\text{m}^2])^{-1/2}$ is taken from (4). For the Brillouin simulations, we used $m_i/(Zm_e) = 1836$, a plasma density $n_e = 0.3n_{cr}$ and pump amplitudes $a_0 = 0.0085, 0.027$ and 0.085 , corresponding to $10^{14}, 10^{15}$ and 10^{16} W cm⁻², and pump pulse durations of 11.4 ps, 3.8 ps and 1.1 ps respectively. We use $\tau_1(0)/\tau_B = 0.1, 0.2, 0.5, 1.0, 2.0$ and 5.0 , where $\tau_B[\text{s}] = 1.78 \times 10^{-9} \lambda_0[\mu\text{m}][(Zm_e/m_i)(n_e/n_{cr})(1 - n_e/n_{cr})(I_1 \lambda_1^2[\text{Wcm}^{-2}\mu\text{m}^2])]^{-1/3}$ is taken from (9). The parameters of the simulations are discussed at length in the Supplementary Information [47].

In Figure 1, we show the evolution of $\omega_0\tau_1$ versus a_1 for simulations of Raman (left) and Brillouin (right) amplification, to demonstrate the ‘‘attractor’’ nature of the optimal seed pulse solutions (4) and (9). The dashed lines in each frame represent Eqns. (4) and (9) evaluated for these cases. The top two frames show $(\omega_0\tau_1, a_1)$ for various initial pump and seed pulse intensities, where $\tau_1(0) = \tau_R$ or $\tau_1(0) = \tau_B$ in each simulation. We find that the evolving seed pulses closely follow the analytical predictions, irrespective of the pump

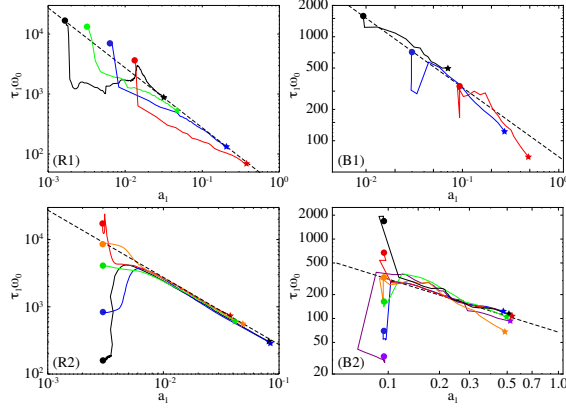


Figure 1: Evolution of duration (τ_1) versus peak amplitude (a_1) of Raman (R1,R2) and sc-Brillouin (B1,B2) amplified pulses for different pump amplitudes (R1,B1) or initial seed durations (R2,B2), demonstrating the attractor nature of the ideal solutions. R1: $n_0/n_{cr} = 0.0044$, and $a_0/a_{wb} = 0.25$ (black), 0.5 (green), 1.0 (blue) and 2.0 (red), with initial seed amplitude $a_1 = a_0$ for each case. B1: $n_0/n_{cr} = 0.3$, and $a_0 = 0.0085$ (black), 0.027 (blue) and 0.085 (red); again, $a_1 = a_0$. R2: $n_0/n_{cr} = 0.0044$, $a_1 = a_0 = 0.75a_{wb}$. The initial durations of the seed pulse are $\tau_1/\tau_R = 0.02$ (black), 0.1 (blue) 0.5 (green), 1.0 (orange) and 2.0 (red). B2: $n_0/n_{cr} = 0.3$, and pump and seed amplitudes of $a_0 = a_1 = 0.085$. The initial durations of the seed pulse are $\tau_1/\tau_B = 0.1$ (purple), 0.2 (blue), 0.5 (green), 1.0 (orange), 2.0 (red), and 5.0 (black). The dashed lines correspond to Eqns. (4) for Raman and (9) for sc-Brillouin respectively.

intensity chosen in the simulations, proving that the predictions by (4) and (9) for Raman or Brillouin amplification represent “attractor” solutions and remain valid over a wide range of pulse intensities. For $a_1(t)$ and $\tau_1(t)$, we find that $a_1(t) \propto t$ and $\tau_1(t) \propto 1/t$ for Raman amplification and $a_1(t) \propto t^{3/4}$ and $\tau_1(t) \propto t^{-1/2}$ for sc-Brillouin, although minor aberrations from these scalings were found at the highest pulse intensities due to non-linear effects not covered by the three-wave models, e.g. when the seed pulse becomes powerful enough to drive a wakefield. The bottom two frames show $(\omega_0\tau_1, a_1)$ for fixed pulse intensities, while the initial pulse duration was moved away from the analytical predictions. We find that in each case the seed pulse first evolves until the pair $(\omega_0\tau_1, a_1)$ matches (4) or (9), and then amplifies as dictated by these equations. This specific behaviour was found in all our simulation results, irrespective of the plasma density or pump pulse intensity we used. This proves the following: (i) the π -pulse solution for Raman and its Brillouin equivalent are

indeed attractors, as predicted [15, 16], and (ii) changing the initial seed pulse duration has no significant effect on the end result, so $\tau_1(0)$ should not be treated as a free parameter. The free parameters for both Raman and Brillouin amplification are the pump wave length λ_0 and the density ratio n_0/n_{cr} ; once these two are chosen, the position of the attractor (τ_1, a_1) curve is completely determined by (4) or (9). The intensities of the pulses determine the speed at which the seed pulse evolves, but not the trajectory of $(\tau_1(t), a_1(t))$.

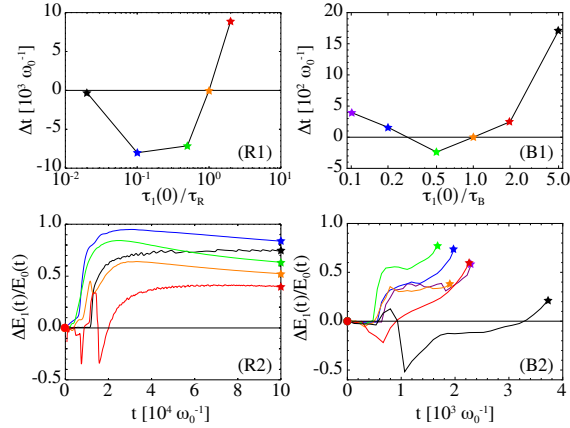


Figure 2: (R1,B1): temporal delay Δt in reaching a given intensity amplification level ($25 \times I_{\text{pump}}$) for seed pulses with various initial durations, for the same cases as shown in frames (R2,B2) of Figure 1. (R2,B2): efficiency of the amplification process for these same cases; ΔE_1 is the seed energy gain, E_0 is the absorbed pump energy.

In Figure 2(R1,B1), we show the time needed for seed pulses with different initial durations to reach a given intensity ($25 \times I_{\text{pump}}$), for the same cases as shown in frames (R2,B2) of Figure 1. We find that amplification is optimal when $0.2 < \tau_1(0)/\tau_{R,B} < 0.5$, ($\tau_{R,B}$ given by (4) or (9)) while significant delays are incurred for $\tau_1(0)/\tau_{R,B} > 1$ or < 0.2 . In Figure 2(R2,B2) we show the efficiency of the amplification process for these same cases ($\Delta E_1 \equiv E_1(t) - E_1(0)$, so $\Delta E_1 < 0$ means that the seed pulse is losing energy rather than gaining). Unsurprisingly, a longer delay in amplification is always accompanied by a lower efficiency. For Raman amplification in particular, we also find that (i) the asymptotic efficiency is mostly constant, (ii) the cases showing the longest delay also exhibit the lowest asymptotic efficiency. This corresponds to the notion that the Raman efficiency is $\eta \approx 4.4/\xi_M$ (see above) and that ξ_M increases for non-ideal initial seed pulses that incur longer delays, in line with predictions for ξ_M in Ref. [15]. So a poorly chosen initial seed

pulse duration will affect the entire amplification process, not just the initial stages. Also, the longest delays correspond to an interaction length of several mm, longer than what is used in many experiments [27, 48–50]. This highlights the need to choose the initial seed pulse parameters according to Eqns. (4) and (9).

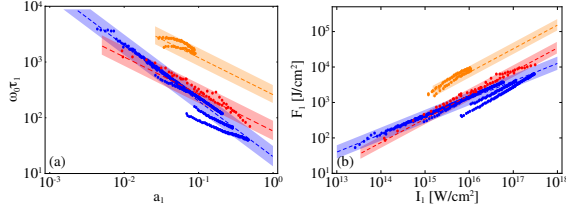


Figure 3: Left: map of (a_1, τ_1) of successfully amplified seed pulses via Raman amplification (blue), sc-Brillouin amplification at over-quarter-critical densities (red) and sc-Brillouin amplification at sub-quarter-critical densities (orange). The points are taken from 1-D PIC simulations while the shaded areas indicate predictions by Eqns. (4) and (9). Right: The same data shown on the left is presented in a map of seed fluence versus seed intensity, for 1 μm pump pulse wave length.

To make the connection with past Raman or Brillouin amplification experiments, we have applied our findings to the initial conditions of various Raman [27, 48–50] and Brillouin amplification experiments [51, 52]. For the initial seed pulses in the Raman experiments, we find that $\Gamma_R a_1 \tau_1 = 0.13$ [27, 48], 0.22 [49], or 0.86 [50], well below our value of 3.4. For the Brillouin experiments, we find that $\Gamma_{sc}^3 a_1^2 \tau_1^3 = 8.6$ [51] or 1.31 [52] again below our value of 13.8. Interestingly, the output pulse after the first pass of the experiments by Ren *et al.* [27, 48] has $\Gamma_R a_1 \tau_1 \approx 3.5$, matching our predictions. Thus, future experiments need either more powerful seed pulses (up to two orders of magnitude extra power for Raman and one order for Brillouin, for similar duration) or longer interaction distances, to allow the pulses time to reshape themselves. We also note that the experiments with the biggest energy gain, Refs. [48, 51] are also the ones using pulses that match our predictions most closely.

In Figure 3, we compare 1-D simulations of Raman amplification at $0.0025 < n_0/n_{cr} < 0.01$ (blue) and sc-Brillouin amplification at $m_i/(Zm_e) = 1836$, $0.275 < n_0/n_{cr} = 0.325$ (red) and $0.0075 < n_0/n_{cr} = 0.0125$ (orange). The density ranges have been chosen to minimize the impact of unwanted instabilities [39]. The dots mark the simulation results, while the shaded areas mark the predictions by Eqns. (4) and (9). The left frame shows τ_1 versus a_1 for the amplified seed; the right frame shows the energy flux $F_1 = I_1 \tau_1$ versus

intensity I_1 for the same cases. All simulation points lie within the theoretically predicted shaded regions, highlighting the robustness of (4) and (9) for a broad range of parameters. Note that Raman and high-density sc-Brillouin produce the shortest pulses and highest intensities. Low-density Brillouin amplification reaches lower peak intensities but yields the highest pulse fluence because of longer pulse durations. These results serve as an important guide when choosing not only the laser and plasma parameters, but also the preferred amplification scheme when designing an experiment to obtain a desired output pulse.

Finally, we applied our findings to the results of previously published 2-D Raman and Brillouin simulations [39, 53], where both the seed pulse amplitude and duration depend on the transverse coordinate r . We found that even if $a_1(r)$ and $\tau_1(r)$ depend on r individually, they still obey Eqns. (4) and (9). For example, for seed pulses with a Gaussian envelope, $a_1(x_2) \propto \exp(-r^2/w_0^2)$, this results in a horseshoe envelope $\tau_1(r) \propto \exp(r^2/w_0^2)$, as seen in Refs. [18, 33–40]. For donut-shaped seed pulses with orbital angular momentum, this even results in a “double horseshoe” envelope [53]. These findings are discussed at length in the Supplementary Material [47]

We have explored the full non-linear evolution of the seed pulse in Raman and Brillouin amplification, and derived essential criteria governing $a_1(t)$ and $\tau_1(t)$, in particular specific products of a_1 and τ_1 that are independent of the pump pulse properties. We have proved the validity of these criteria in 1-D and 2-D particle-in-cell simulations. Furthermore, we have demonstrated the importance of choosing the initial seed duration wisely: a non-optimal value for this parameter (far from the ideal attractor solution) will delay amplification of the seed pulse and reduce efficiency. In relation to experiments on parametric amplification, our results provide unique criteria for their design, and novel predictions for the properties of the amplified seed pulse, and advice on which scheme to choose to obtain the desired end result. Since the ideal amplified seed pulse assumes the shape of a cnoidal wave [2, 15, 16], our results also explain the “bursty behaviour” observed in Brillouin scattering [54, 55], as the scattered radiation assumes a very similar shape. Since the equations for Raman scattering in solid-state physics or non-linear optics have a shape similar to Eqns. (1)-(2) (see Refs. [2–8]) our results will be useful for Raman and Brillouin scattering in general (not just in plasma), or to any optical three-wave process with Kerr or $\chi^{(3)}$ non-linearity and counter-propagating pulses, ensuring a wide range of applications.

This work has been carried out within the framework of the EUROfusion Consortium and

has received funding from the Euratom research and training programme 2014-2018 under grant agreement No. 633053. The views and opinions expressed herein do not necessarily reflect those of the European Commission. The authors acknowledge financial support from STFC, from the European Research Council (ERC-2010-AdG Grant 167841), from FCT (Portugal) grant No. SFRH/BD/75558/2010 and from LaserLab Europe, grant no. GA 654148. We acknowledge PRACE for providing access to resources on SuperMUC (Leibniz Supercomputing Centre, Garching, Germany).

Parameters of the numerical simulations. For the simulations in the main manuscript, we have used the particle-in-cell codes XOOPIC [45] and OSIRIS [46]. The parameters are discussed in detail here. We distinguish numerical parameters (spatial resolution, time step, number of particles per grid cell) and physical parameters (laser pulse duration, spot diameter and amplitude, plasma density, plasma species, laser-plasma interaction length, etc.)

Both the Raman and Brillouin runs that have been performed with for figures 1 and 2 of main manuscript have been done using a moving simulation window. This window followed the seed pulse, while the pump pulse was brought into the simulation box via a time-dependent boundary condition.

The numerical parameters were as follows. For the Raman runs (frames R1 and R2 in both figures of the main manuscript), the spatial resolution was 50 points per pump laser wavelength (i.e. $dx = 21$ nm). The time step was given by $dt = 0.95dx/c$. The number of particles was 100 particles per cell per species. The interpolation between particles and grid was done using quadratic splines. Ions were treated as an immobile background. For the Brillouin runs (frames B1 and B2 in both figures of the main manuscript), the spatial resolution was $dx = 0.5\lambda_D$, where λ_D is the Debye length. This corresponds to about 220 points per pump laser wavelength (i.e. $dx = 4.8$ nm). The time step was again $dt = 0.95dx/c$. The number of particles was again 100 particles per cell per species, and cubic splines were used for interpolation.

The physical parameters were as follows. The pump laser wave length was $1 \mu\text{m}$ for both the Raman and Brillouin simulations. The seed laser wave length for the Raman simulations was $1.07 \mu\text{m}$, chosen to ensure that $\omega_1 = \omega_0 - \omega_{pe}$. The seed laser wave length for the Brillouin runs was $1 \mu\text{m}$. (This hardly matters since the frequency difference between pump and seed

pulses in Brillouin amplification is considerably less than the seed pulse bandwidth.) For the Brillouin runs in figure 1, frames B1, the interaction length was about $2 \times 10^4 c/\omega_0$, $8 \times 10^3 c/\omega_0$, and $2 \times 10^3 c/\omega_0$ for the simulations with pump intensity 10^{14} , 10^{15} and 10^{16} W/cm² simulations of frame B1. The interaction lengths for the simulations in figure 1, frame B2, are $2 \times 10^3 c/\omega_0$ in each case. This corresponds to an interaction distance of 335 micron, or a 2.2 ps pump pulse duration. The interaction distance for the Raman runs in figure 1 was up to $10^5 c/\omega_0$ or up to 16 mm in each case.

The interaction distance for the simulations displayed in figure 2 is up to $10^5 c/\omega_0$ for the Raman runs, and up to $2 \times 10^3 c/\omega_0$ for the Brillouin runs.

The plasma density was chosen to be $n_e = n_{cr}/225$ for the Raman simulations, and $n_e = 0.3n_{cr}$ for the Brillouin simulations. The plasma electron temperature was chosen to be 1 eV for the Raman simulations and 500 eV for the Brillouin simulations.

Transverse effects. In a multi-dimensional setting, the amplitude a_1 and duration τ_1 of the growing seed laser pulse will of course depend on the transverse coordinate x_2 . The same holds true for the location of the seed pulse maximum, τ_M . This leaves an imprint on the full shape of the envelope when parametric amplification is studied in more than one dimension.

From Equations (4) and (9), we find that the x_2 -dependence of the amplitude a_1 also induces an x_2 -dependence of the duration τ_1 , even for fixed t . For example, for seed pulses with a Gaussian envelope, $a_1(x_2) \propto \exp(-x_2^2/w_0^2)$, this results in a horseshoe envelope $\tau_1(x_2) \propto \exp(x_2^2/w_0^2)$ [18, 33–40]. For donut-shaped seed pulses with orbital angular momentum, this even results in a “double horseshoe” envelope [53]. We will verify such horseshoe seed pulse shapes against Eqns. (4) and (9) here.

In Figure 4, we verify the horseshoe shape of seed pulses after amplification. Here, we present the analysis of a 2-D Raman simulation (R), taken from Ref. [39], Figure 2a, a 3-D Raman simulation with orbital angular momentum and a doughnut-shaped seed pulse intensity envelope (OAM), taken from Ref. [53], Figure 1a and 2a, and a 2-D sc-Brillouin simulation (B), using $m_i/(Zm_e) = 1836$, $n_0/n_{cr} = 0.3$ and $a_0 = 0.027$. Frames R1, OAM1 and B1 show the vector potential envelopes for these pulses. Frames R2, OAM2 and B2 show $a_1(x_2)$, $\omega_0\tau_1(x_2)$ and $\Gamma_R a_1(x_2)\tau_1(x_2)$ and $A\Delta\xi \approx 3.4$ (R2,OAM2) or $\Gamma_{sc}^3 a_1^2(x_2)\tau_1^3(x_2)$ and $A^2\Delta\xi^3 \approx 13.8$ (B2), all versus transverse coordinate x_2 . In all cases, the curved shape of the seed pulse is well described by Eqns. (4) or (9). Even for strange pulse envelope shapes,

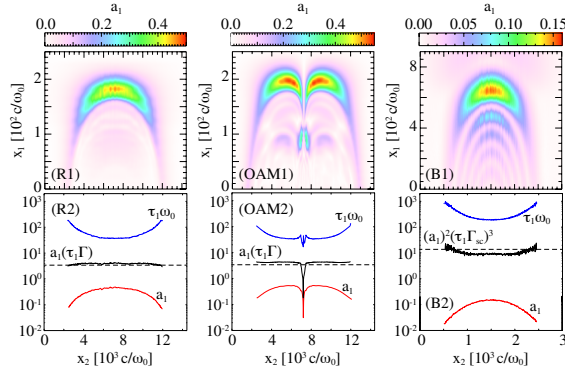


Figure 4: Analyzing the curved shape of the amplified seed pulse for Raman (R) and Raman with OAM (OAM) and Brillouin (B) amplification in multi-dimensional simulations. The top frames show the amplitude envelopes of the amplified seeds. The bottom frames show $a_1(x_2)$ (red) and $\omega_0\tau_1(x_2)$ (blue) versus the transverse coordinate x_2 . The products $a_1(x_2)\Gamma_R\tau_1(x_2)$ (R,OAM) and $a_1^2(x_2)[\Gamma_{sc}\tau_1(x_2)]^3$ (B), given by black curves, are then verified against Eqns.(4) and (9) (dashed lines).

like the “donut” shape of the pulse with OAM, the relationships between pulse amplitude and duration still hold. The presence or absence of parasitic instabilities does not have much of an influence on this behaviour. For example, in Ref. [39], one can see numerical simulations of two Raman-amplified laser pulses, one with and one without filamentation. Both pulses exhibit the horseshoe shape predicted here.

-
- [1] C.V. Raman, Ind. J. Phys., **2**, 387 (1928); C.V. Raman and K.S. Krishnan, Ind. J. Phys., **2**, 399 (1928).
 - [2] J. A. Armstrong, N. Bloembergen, J. Ducuing, and P. S. Pershan, Phys. Rev. **127**, 1918 (1962).
 - [3] Y.R. Sen and N. Bloembergen, Phys. Rev. **137**, A1787 (1965).
 - [4] Flora Y. F. Chu and Alwyn C. Scott, Phys. Rev. A **12**, 2060 (1975).
 - [5] D. J. Kaup, A. Reiman and A. Bers, Rev. Mod. Phys. **51**, 275 (1979).
 - [6] C. R. Menyuk, D. Levi, and P. Winternitz, Phys. Rev. Lett. **69**, 3048 (1992).
 - [7] G. Lamb Jr., Phys. Lett. A **25**, 181 (1967).
 - [8] G. Lamb Jr., Phys. Lett. A **29**, 507 (1969).

- [9] D.W. Forslund, J.M. Kindel and E.L. Lindman, Phys. Fluids **18**, 1002-1016 (1975).
- [10] M. Maier, W. Kaiser, and J. A. Giordmaine, Phys. Rev. Lett. **17**, 1275 (1966).
- [11] R. D. Milroy, C. E. Capjack, and C. R. James, Plasma Phys. **19**, 989, (1977).
- [12] R. D. Milroy, C. E. Capjack, and C. R. James, Phys. Fluids **22**, 1922 (1979).
- [13] C. E. Capjack, C. R. James, and J. N. McMullin, J. Appl. Phys. **53**, 4046 (1982).
- [14] A.A. Andreev and A.N. Sutyagin, Kvant. Elektron. **16**, 2457 (1989) [Sov. J. Quantum Electron. **19**, 1579 (1989)].
- [15] V.M. Malkin, G. Shvets and N.J. Fisch, Phys. Rev. Lett. **82**, 4448 (1999).
- [16] A.A. Andreev *et al.*, Phys. Plasmas **13**, 053110 (2006).
- [17] G. Shvets, N. J. Fisch, A. Pukhov and J. Meyer-ter-Vehn, Phys. Rev. Lett **81**, 4879 (1998).
- [18] I. Y. Dodin, G. M. Fraiman, V. M. Malkin, and N. J. Fisch, Zh. Eksp. Teor. Fiz. **122**, 723 (2002) [JETP **95**, 625 (2002)].
- [19] N. J. Fisch and V. M. Malkin, Phys. Plasmas **10**, 2056 (2003).
- [20] Y. Ping, W. Cheng, S. Suckewer, D.S. Clark, N.J. Fisch, Phys. Rev. Lett. **92**, 175007 (2004).
- [21] B. Ersfeld and D.A. Jaroszynski, Phys. Rev. Lett. **95**, 165002 (2005).
- [22] J. Kim, H.J. Lee, H. Suk and I.S. Ko, Phys. Lett. A **314**, 464 (2003).
- [23] V. M. Malkin, G. Shvets, and N. J. Fisch, Phys. Rev. Lett. **84**, 1208 (2000).
- [24] Yu. A. Tsidulko, V. M. Malkin and N. J. Fisch, Phys. Rev. Lett. **88**, 235004 (2002).
- [25] W. Cheng, *et al.*, Phys. Rev. Lett. **94**, 045003 (2005).
- [26] N. A. Yampolski *et al.*, Phys. Plasmas **15**, 113104 (2008).
- [27] J. Ren *et al.*, Phys. Plasmas **15**, 056702 (2008).
- [28] V. M. Malkin and N. J. Fisch, Phys. Rev. Lett. **99**, 205001 (2007).
- [29] V. M. Malkin, G. Shvets, and N. J. Fisch, Phys. Plasmas **7**, 2232 (2000).
- [30] N. A. Yampolsky, V. M. Malkin, and N. J. Fisch, Phys. Rev. E **69**, 036401 (2004).
- [31] G. Lehmann, K. H. Spatschek, and G. Sewell, Phys. Rev. E **87**, 063107 (2013).
- [32] G. Lehmann and K. H. Spatschek, Phys. Plasmas **20**, 073112 (2013).
- [33] R.M.G.M. Trines, *et al.*, Phys. Rev. Lett. **107**, 105002 (2011).
- [34] P. Mardahl *et al.*, Phys. Lett. A **296**, 109 (2002).
- [35] G. M. Fraiman, N. A. Yampolsky, V. M. Malkin, and N. J. Fisch, Phys. Plasmas **9**, 3617 (2002).
- [36] A. A. Balakin, G. M. Fraiman, N. J. Fisch, and V. M. Malkin, Phys. Plasmas **10**, 4856 (2003).

- [37] A. A. Balakin *et al.*, IEEE Trans. Plasma Sci. **33**, 488489 (2005).
- [38] M. S. Hur and J. Wurtele, Comp. Phys. Comm. **180**, 651 (2009).
- [39] R. M. G. M. Trines *et al.*, Nature Physics **7**, 87 (2011).
- [40] G. Lehmann and K. H. Spatschek, Phys. Plasmas **21**, 053101 (2014).
- [41] B.I. Cohen and C.E. Max, Physics of Fluids **22**, 1115 (1979).
- [42] B.I. Cohen *et al.*, Phys. Plasmas **8**, 571 (2001).
- [43] E.A. Williams *et al.*, Phys. Plasmas **11**, 231 (2004).
- [44] S. Hüller, P. Mulser and A. M. Rubenchik, Phys. Fluids B **3**, 3339 (1991).
- [45] J.P. Verboncoeur, A.B. Langdon, and N.T. Gladd, Comput. Phys. Commun. **87**, 199 (1995).
- [46] R.A. Fonseca *et al.*, Lect. Notes Comp. Sci. **2331**, 342 (2002).
- [47] Supplementary Information accompanying this paper at <http://journals.aps.org/prl/>
- [48] J. Ren *et al.*, Nature Physics **3**, 732-736 (2007).
- [49] R. Kirkwood *et al.*, Phys. Plasmas **14**, 113109 (2007).
- [50] Y. Ping *et al.*, Phys. Plasmas **16**, 123113 (2009).
- [51] L. Lancia, *et al.*, Phys. Rev. Lett. **104**, 025001 (2010).
- [52] L. Lancia, *et al.*, Phys. Rev. Lett. **116**, 075001 (2016).
- [53] J. Vieira, R.M.G.M. Trines *et al.*, Nature Communications **7**, 10371 (2016).
- [54] C. Riconda *et al.*, Phys. Plasmas **13**, 083103 (2006).
- [55] C. Riconda *et al.*, Phys. Plasmas **18**, 092701 (2011).